 doi:10.20944/preprints202104.0573.v1

Article

A surgical pen-type probe design for real-time optical diagnosis of tumor status using 5-aminolevulinic acid

Ki-cheol Yoon[1,2], Kwang Gi Kim[1,2,3,4,*], and Seung Hoon Lee[5,6],

[1]Dept. of Biomedical Engineering, College of Medicine, Gachon University, 38-13, Dokjom-ro 3, Namdong-gu, Incheon 21565, Republic of Korea; kcyoon98@gachon.ac.kr
[2]Medical Devices R&D Center, Gachon University Gil Hospital, 21, 774 beon-gil, Namdong-daero Namdong-gu, Incheon 21565, Republic of Korea
[3]Dept. of Biomedical Engineering, College of Health Science, Gachon University, 191 Hambakmoero, Yeonsu-gu, Incheon 21936, Republic of Korea;
[4]Dept. of Health Sciences and Technology, Gachon Advanced Institute for Health Sciences and Technology (GAIHST), Gachon University, 38-13, 3 Dokjom-ro, Namdong-gu, Incheon 21565, Republic of Korea
[5]Dept. of Neurosurgery, Daejeon Eulji Medical Center (Eulji Univ. Hospital), Dunsanseo-ro, Seo-gu, Daejeon, 35233 Republic of Korea
[6]School of Medicine, Eulji University, 77 Gyeryong-ro 771 Beon-gil, Jung-gu Daejeon 34824 Republic of Korea
* Correspondence: kimkg@gachon.ac.kr; Tel.: +82-32-458-2770

Abstract: A surgical microscope is large in size, which makes it impossible to be portable. The distance between the surgical microscope and the observation tissue is 15–30 cm, and the adjustment range of the right and left of the camera is a maximum of 30°. Therefore, the surgical microscope is generated attenuation (above 58%) of irradiation optical source owing to the long working distance. Moreover, the observation of tissue is affected because of dazzling by ambient light as the optical source power is strong (55 to 160 mW/cm^2). Further, observation blind spot phenomena will occur due to the limitations in adjusting the right and left of the camera. Therefore, it is difficult to clearly observe the tumor.

In this study, a compact pen-type probe with a portable surgical microscope is presented. The proposed surgical microscope comprises a small and portable pen-type probe that can adjust the working distance between the probe and the observed tissue. In addition, it allows the adjustment of the viewing angle and fluorescence brightness. The proposed probe has no blind spots or optical density loss.

Keywords: fluorescence microscopy; fluorescence emission, malignant tumor, diagnosis, animal experiment

1. Introduction

The 5-aminolevulinic acid (5-ALA) fluorescence dye is used to assess the condition of tumor removal in gliomas, brain cancer, breast cancer, colonic mucosa, and ovarian cancer [1]-[5]. In particular, malignant tumors are complex and composed of tumors and blood vessels. Tumors and vasculature have the same color, making it difficult to differentiate the boundary between them using the naked eye. Hence, surgical observation systems [2], such as surgical computed tomography (CT), surgical navigators, magnetic resonance imaging (MRI), positron emission tomography (PET), ultrasonography, and surgical microscopes [6]-[12], are used in cancer surgery.

They mainly produce black and white images. However, it is difficult to determine the size, location, and morphological boundaries of cerebrovascular, lymph node, or malignancies using a surgical microscope, as the image quality is not excellent because the image is black and white [8]. To address this, a surgical color camera can be used. Surgical color cameras clearly show the color of the vasculature and tumor. However, because tumors and blood vessels have the same shape and color, it is difficult to distinguish and observe them using color cameras [13].

Therefore, a fluorescence observation module can be connected to a surgical color-imaging camera. When used in surgery, fluorescent image guidance cameras for surgery can distinguish the shape, color, and boundaries of tumors and blood vessels because of their fluorescence expression

Preprints (www.preprints.org) | NOT PEER-REVIEWED | Posted: 21 April 2021 doi:10.20944/preprints202104.0573.v1

[8], [14]. However, these guidance cameras have disadvantages as they are large and heavy (camera head: above 4 kg, entire: above 6 kg) with limited portability [15]-[21]. In addition, they allow limited adjustment of the observed beam angles (maximum 30°) and working distances of 15–30 cm/cm^2 [15]-[24]. Because a surgical camera uses a high-energy light source (55–160 mW/cm^2) for the electromotive force of fluorescence emission, optical source beam energy loss (above 58%) can occur at the working distance (15–30 cm), and strong ambient light can be observed around the tissue (photobleaching) [10], [15], [23, 24]. Thus, the surgical microscope is difficult to operate for tissue observation owing of the limitations of beam working distance (WD) control and adjustment of the left and right of the camera [16, 17]. In addition, surgical diagnostic systems are not portable because of their large size [10], [23].

To address the abovementioned problems, this study aimed to develop a pen-type surgical fluorescence microscope that is small and portable with an adjustable beam angle. It provides real-time diagnosis. The performance of the proposed pen-type probe was verified through animal experiments by using a light source of 405 nm and a fluorescence wavelength of 620 to 670 nm.

2. Design of the Pen-type Probe

The conventional surgical microscope (with a laser diode (LD) and near-infrared (NIR) camera) and the proposed pen-type probe are compared in Fig. 1 [18]. Fig. 2 shows the detailed structure of the proposed pen-type probe. As shown in the figure, it comprises a laser diode, a drive module (for laser drive), a small camera module (SE-8J200), a switch (ON/OFF), a laser brightness control performance, a battery, a long-pass filter, and a communication cable. The communication cable connects the camera and the external monitor. Therefore, the videos captured by the camera can be read in real time on an external monitor through a wire.

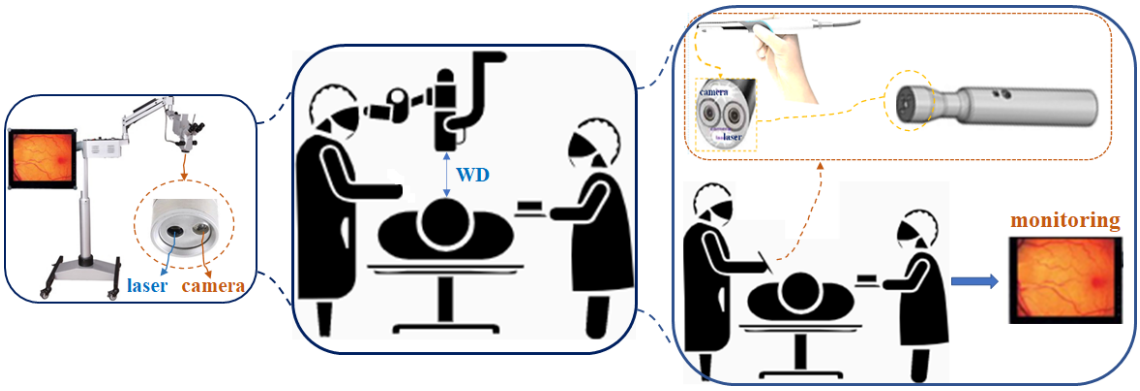

Figure 1. Structure of the conventional surgical microscope and proposed pen-type probe.

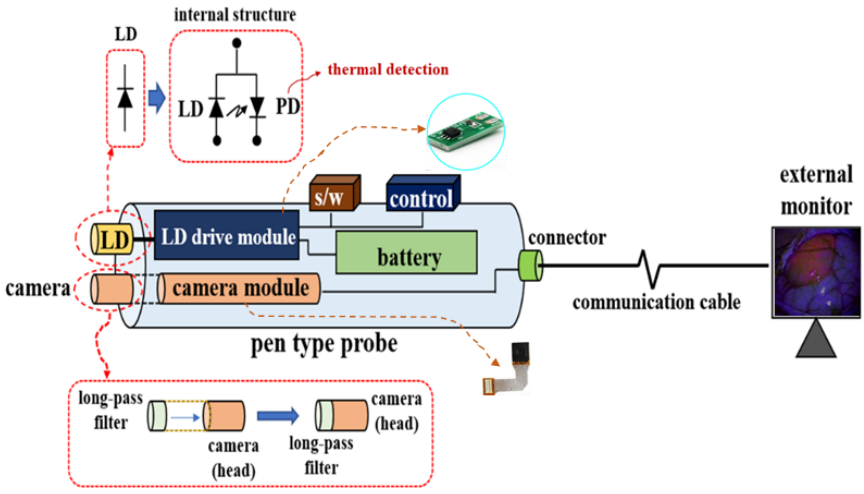

Figure 2. Detailed structure of a proposed pen-type probe.

The LD used was DL-5146-101s from Tholabs, with an excitation wavelength of 405 nm. In the LD drive module, the bias voltage, current, power, and beam divergence (θ_{div}) are 5.6 V, 100 mA, 19 mW/cm^2, and 16°, respectively. The LD's operating voltage (bias voltage) is only 8.0 V. The bias voltages of the LD and drive modules were independent.

Preprints (www.preprints.org) | NOT PEER-REVIEWED | Posted: 21 April 2021 doi:10.20944/preprints202104.0573.v1

The laser brightness control performance was controlled using a variable resistor (max. 10 kΩ). Therefore, the LD can adjust the excitation power. The endoscope camera was used in the CMOS sensor, and the bias voltage of the camera module was 3 V. In addition, the horizontal length and diameter of the camera dimensions were 4 mm and 1.5 mm, respectively, as shown in Fig. 3 (a).

From the figure, the resolution, imaging frame, pixel size, field of view (FOV), and sensor type of the camera were 1600×1200, 30 fps, 2.0 M_{pixel}, 60°, and CMOS sensor type, respectively. The irradiation beam angle of the LD was free degree. In addition, the working distance and beam focus angle (θ_f) of the camera were 50 mm and 9.5°, respectively (see Fig. 1). Then, the working distance was adjusted from 0 to 50 cm, and the realization environment was measured to be 50 mm.

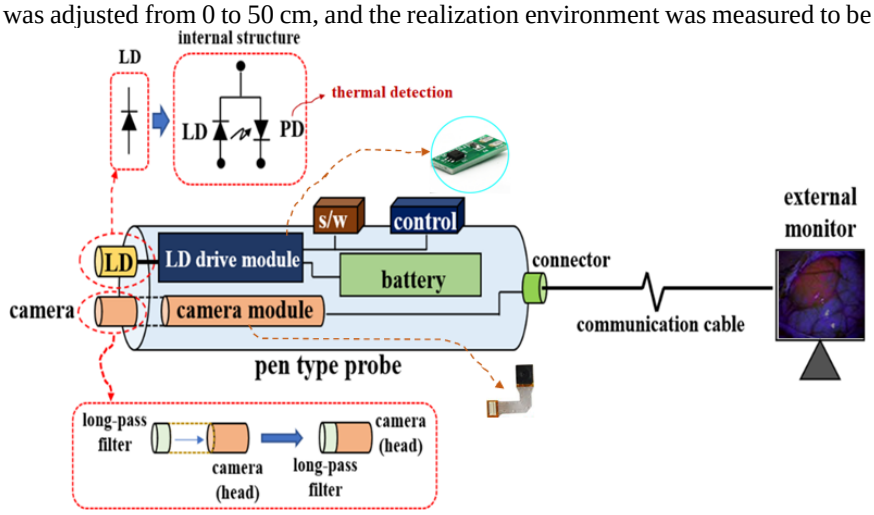

Figure 2. Detailed structure of a proposed pen-type probe.

The LD used was DL-5146-101s from Tholabs, with an excitation wavelength of 405 nm. In the LD drive module, the bias voltage, current, power, and beam divergence (θ_{div}) are 5.6 V, 100 mA, 19 mW/cm^2, and 16°, respectively. The LD's operating voltage (bias voltage) is only 8.0 V. The bias voltages of the LD and drive modules were independent.

The laser brightness control performance was controlled using a variable resistor (max. 10 kΩ). Therefore, the LD can adjust the excitation power. The endoscope camera was used in the CMOS sensor, and the bias voltage of the camera module was 3 V. In addition, the horizontal length and diameter of the camera dimensions were 4 mm and 1.5 mm, respectively, as shown in Fig. 3 (a).

From the figure, the resolution, imaging frame, pixel size, field of view (FOV), and sensor type of the camera were 1600×1200, 30 fps, 2.0 M_{pixel}, 60°, and CMOS sensor type, respectively. The irradiation beam angle of the LD was free degree. In addition, the working distance and beam focus angle (θ_f) of the camera were 50 mm and 9.5°, respectively (see Fig. 1). Then, the working distance was adjusted from 0 to 50 cm, and the realization environment was measured to be 50 mm.

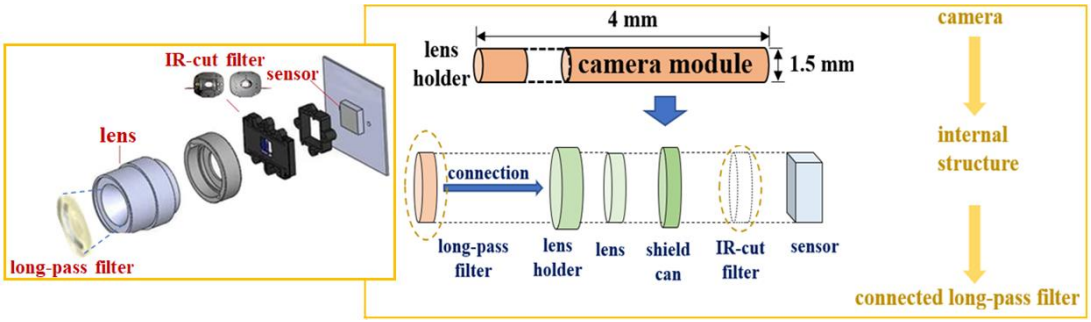

(a)

Preprints (www.preprints.org) | NOT PEER-REVIEWED | Posted: 21 April 2021 doi:10.20944/preprints202104.0573.v1

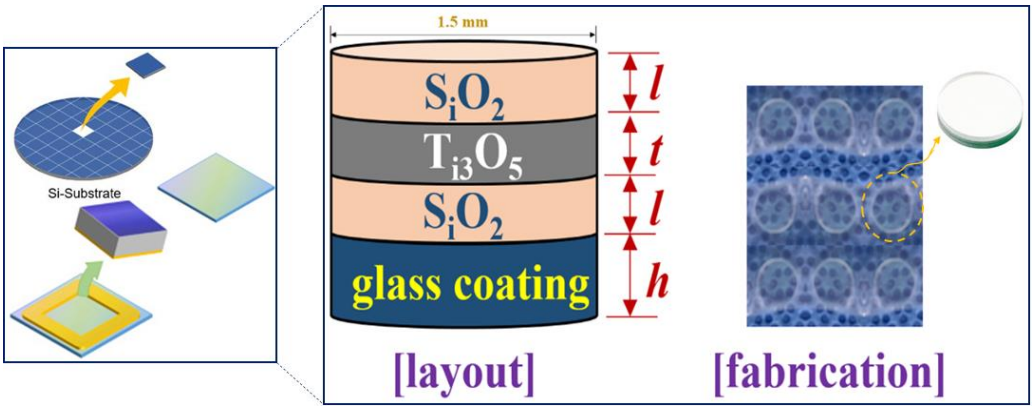

(b)

Figure 3. Photograph of the camera and long-pass filter (a) structure of the connection between to camera module and long-pass filter (b) fabrication of long-pass filter

The camera lens (head) was connected to a long-pass filter with a cut-on wavelength of 600 nm, as shown in Fig. 3 (a). Therefore, the long-pass filter was fabricated using titanium oxide ($T_{i3}O_5$), silicon oxide (S_iO_2), and a glass-coated substrate, as shown in Fig. 3 (b). From the figure, the *t*, *l*, and *h* of the fabricated filter are 2, 4, and 0.4 μm, and the diameter of the filter is 1.5 mm.

The long-pass filter only transmits the emission wavelength of 5-ALA (620–670 nm) fluorescence dye and produces a diagnosis image without any excitation wavelength (405 nm). The pen-type probe was equipped with a low-cost camera. Fig. 4 shows the fabrication of a pen-type probe that was created via the 3 D printing technique.

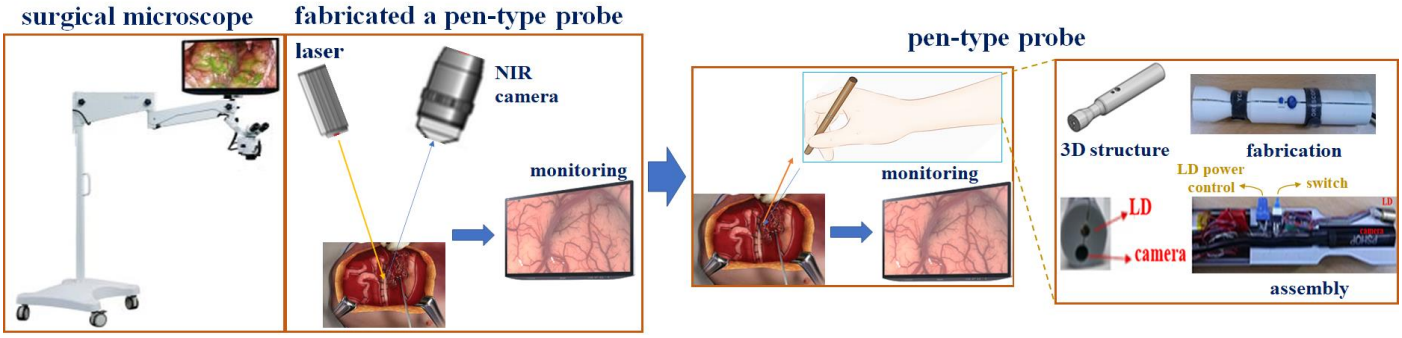

Figure 4. Fabricate a pen-type probe using 3D printing technique.

The overall size and weight of the pen-type probe were 17 mm × 2.5 mm and 32 g (± 2 g), respectively; the weight of the conventional surgical microscope is 6.0 kg [20]- [23]. Thus, the pen-type probe is lighter than the conventional surgical microscope.

3. Experimental Results

The measurement results for the fabrication of the long-pass filter are shown in Fig. 5. From the figure, the cut-in wavelength, transmission (T), and reflection (OD: Optical density) are 600 nm, 98%, and 0.2%, respectively.

Preprints (www.preprints.org) | NOT PEER-REVIEWED | Posted: 21 April 2021 doi:10.20944/preprints202104.0573.v1

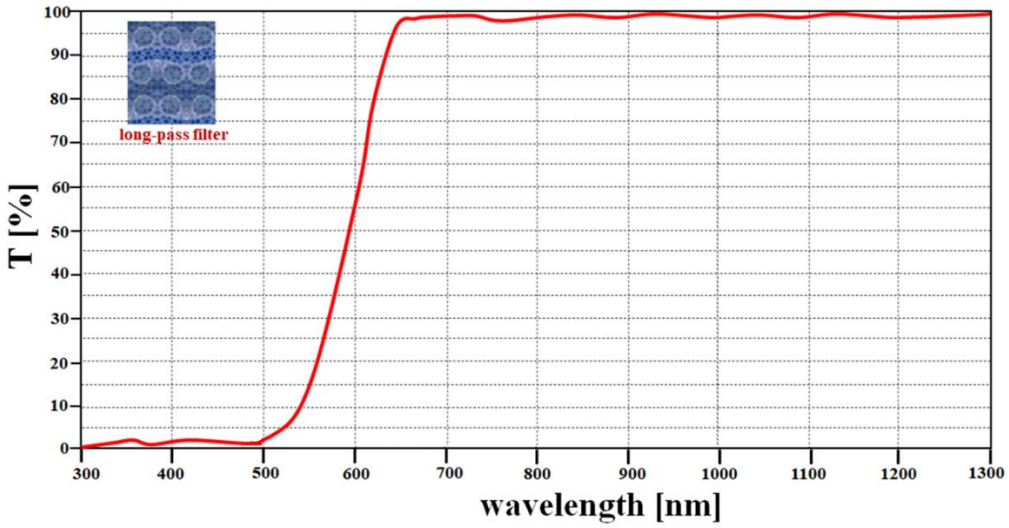

Figure 5. Measurement result of fabricated a long-pass filter

A small animal (rat) experiment was performed to test the performance of the produced pen-type probe. Fig. 6 shows the surgical environment for the animal test. As shown in the figure, the pen-type probe was connected to an external monitor using a cable.

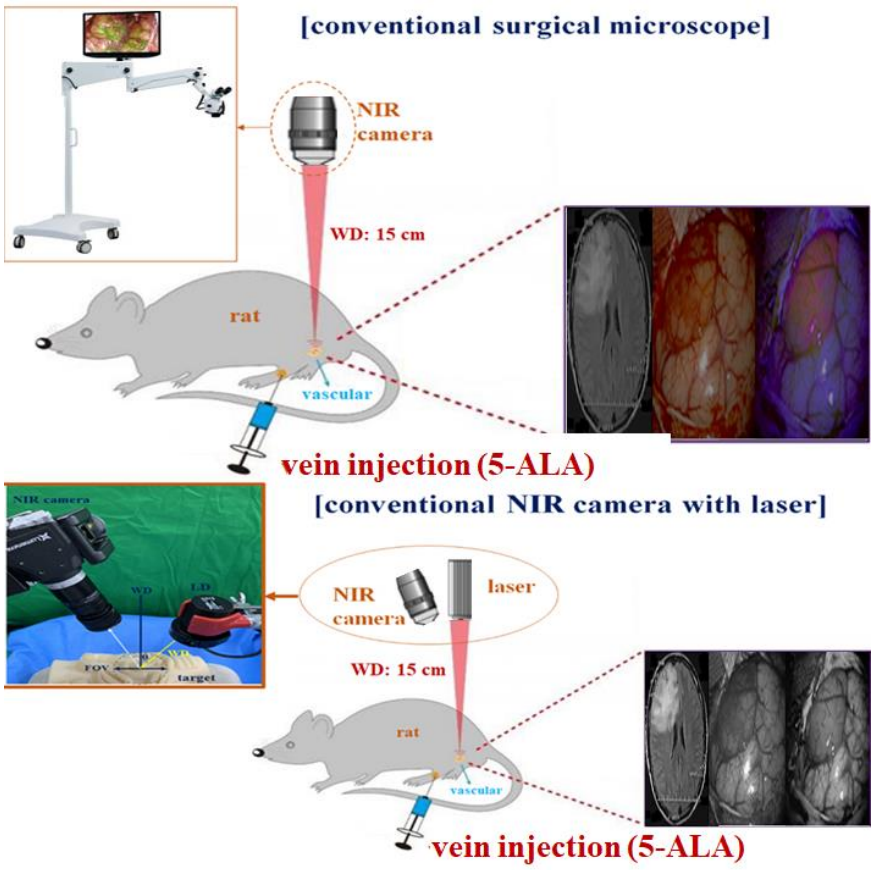

(a)

Preprints (www.preprints.org) | NOT PEER-REVIEWED | Posted: 21 April 2021 doi:10.20944/preprints202104.0573.v1

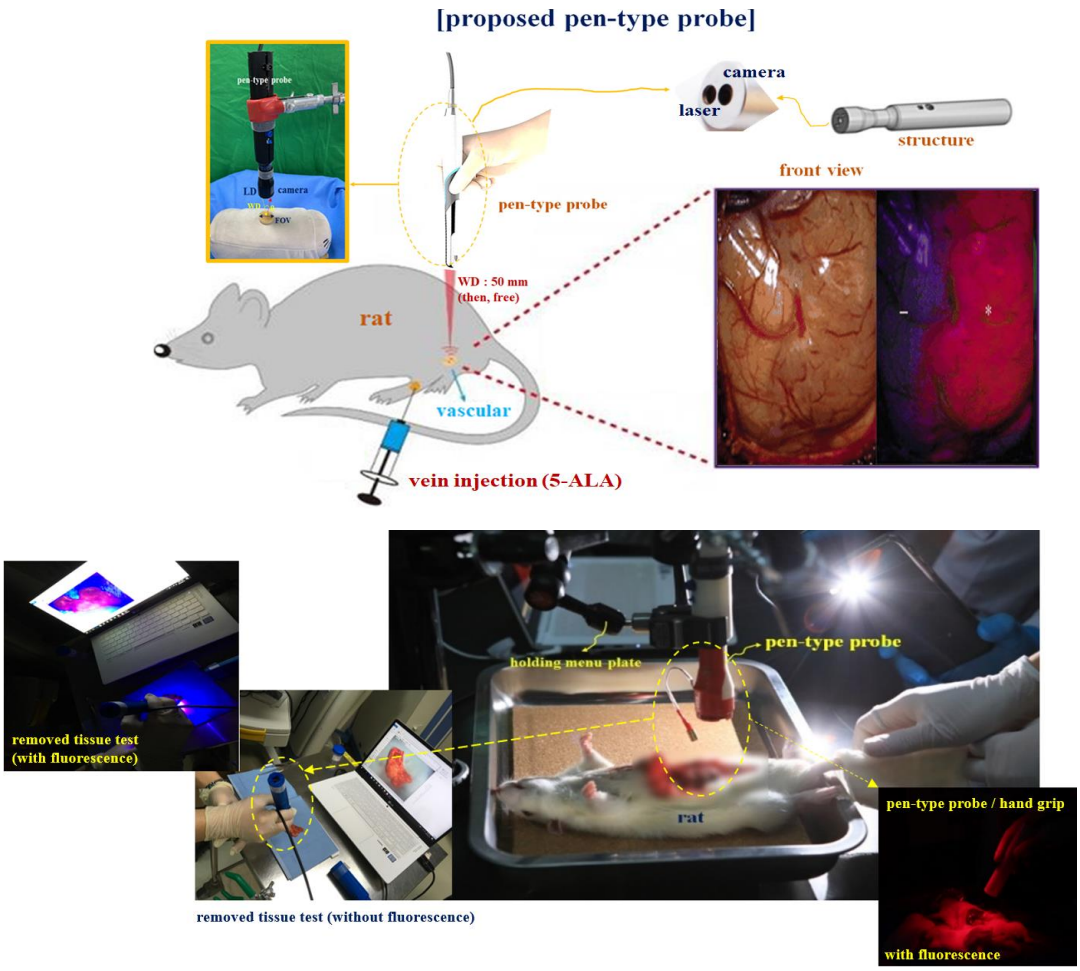

(b)

Figure 6. Rat surgery and small animal test (a) test using conventional surgical microscope and NIR camera with laser (b) pen-type probe test.

The working distance (WD) was determined to be 15 cm (conventional surgical microscope and NIR camera) and 50 mm (pen-type probe). However, the WD of a pen-type probe is free between the distances of 50 mm and 50 cm. In addition, the animal was tested from the Experimental Animal Center of Korea's Lee, Gil-Ya Cancer Diabetes Research Institute; the IACAU number is LCDI-2017-0050. We requested for permission from the animal ethics commission of the animal institutional review board (IRB). The species, age, weight, and strains were rat (male), 8 weeks, 240 g, and Sprague Dawley (SD), respectively. As shown in Fig. 7 (a), a 5-ALA fluorescent contrast agent was injected into the rats. The fluorescence intensity of the fluorescent contrast agent was determined according to the concentration.

(a)

Preprints (www.preprints.org) | NOT PEER-REVIEWED | Posted: 21 April 2021 doi:10.20944/preprints202104.0573.v1

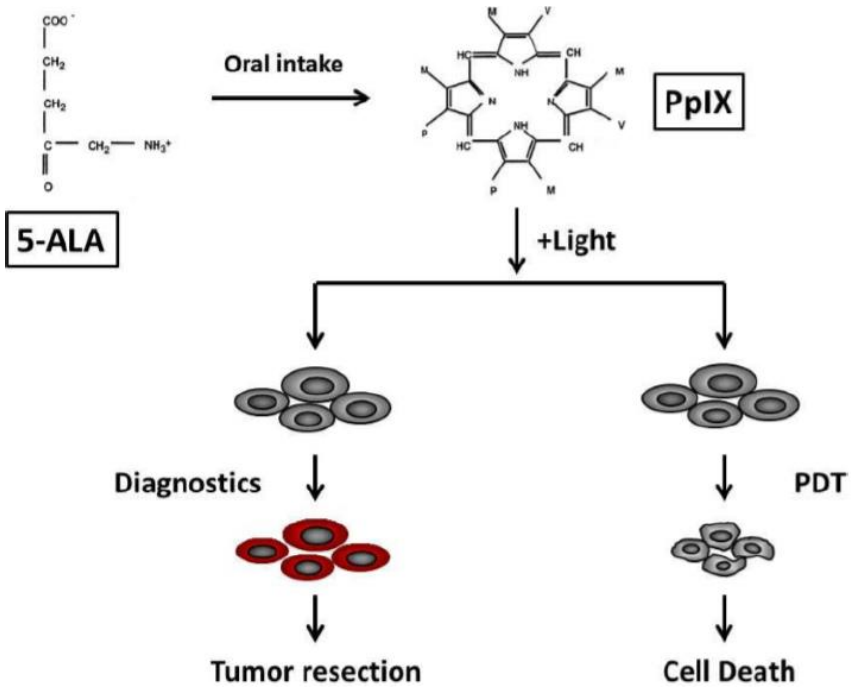

(b)

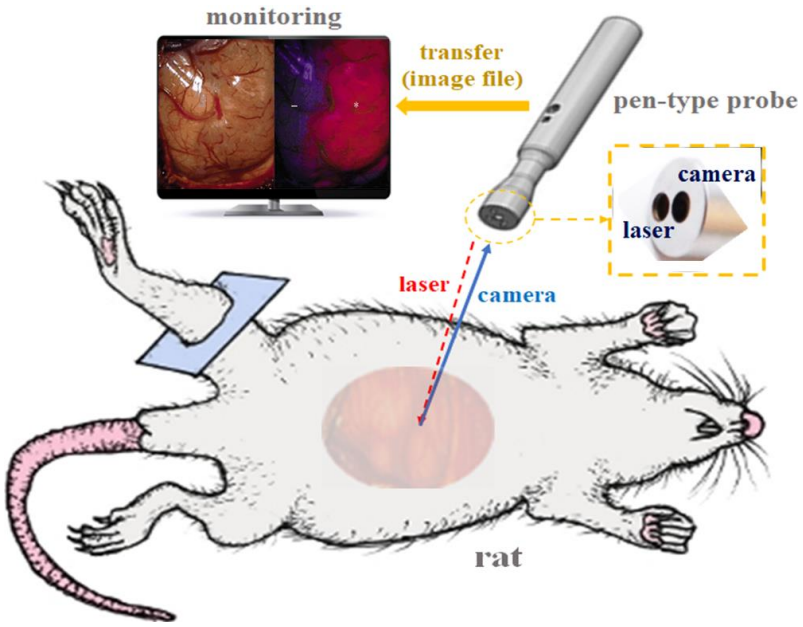

(c)

Figure 7. 5-ALA fluorescence contrast process. (a) process of injection, (b) molecular structure of plasma protein binding by 5-ALA injection, (c) test method.

The fluorescent contrast medium 5-ALA was injected (25 mg/kg @ 0.1 ml in phosphate-buffered saline) 5 to 6 h before surgery (Fig. 7 (a)) [24]. Fluorescent protoporphyrin IX (PpIx) accumulated in the tumor tissue during the 5–6 h interval between injection and surgery (Fig. 7 (b) [24]. For the animal test of 5-ALA fluorescence emission, the optical source of the pen-type probe was irradiated onto the tumor of a rat. Then, the excitation wavelength (λ_{ext}) and power of the laser with a conventional surgical microscope and NIR camera (lumenera's Lt-225 NIR M/N) were 405 nm and 60 mW/cm^2, respectively. The laser (405 nm) used was from PerkinElmer Solaris (optical imaging system) and Thorlabs, M405L2-C1 / MOO47001 (for NIR camera), and the excitation wavelength (λ_{ext}) and power for LD in a pen-type probe were 405 nm and 4 mW/cm^2, respectively.

Preprints (www.preprints.org) | NOT PEER-REVIEWED | Posted: 21 April 2021 doi:10.20944/preprints202104.0573.v1

The LD (Thorlabs DL-5146-101s) power was adjusted from 0 mW/cm^2 to 19.0 mW/cm^2, and the camera was used for SE-8J200 (endoscopy type microscopy).

When the LD of the pen-type probe excites a wavelength of 405 nm (4 mW/cm^2) on the tumor, the fluorescence emitted by the PpI_X in the tumor can be observed by monitoring the state for tumor removal or extant. At this time, the reported fluorescence emission wavelength ranged from 610 to 630 nm [20, 21], [24].

Fig. 8 shows the results of fluorescence emission in tumor removal (or extant) experiments using small animals. This figure shows the state of tumor removal (or extant) through 5-ALA fluorescence in malignant tumors. The fluorescence emission images of tumor removal (or extant) were collected using NIR and infrared cameras. The collected images were observed on a monitor through a cable.

A fluorescent contrast agent with a half-life of 180 min exhibits the liver-uptake phenomenon [24]. The 5-ALA fluorescence has an average 180 min (0.01 mg/kg) liver-uptake phenomenon. The results (see. Fig. 8) show that the pen-type probe's camera can obtain an excellent imaging resolution, similar to that of an NIR camera.

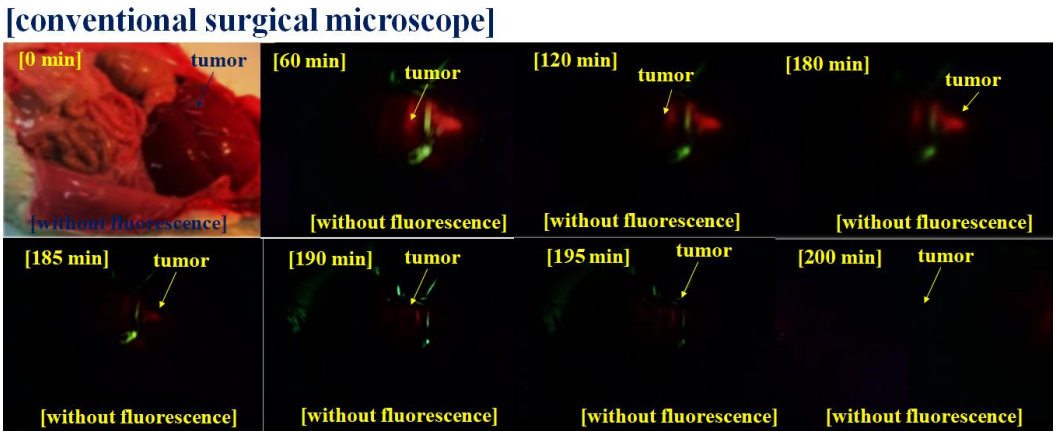

(a)

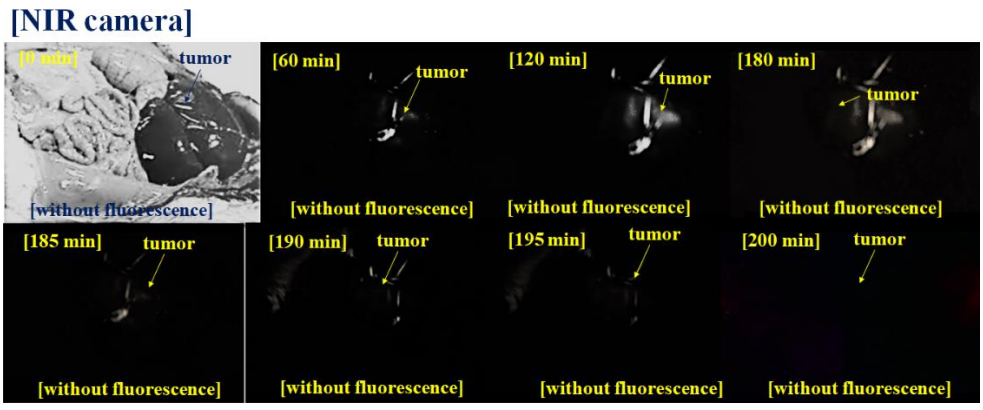

(b)

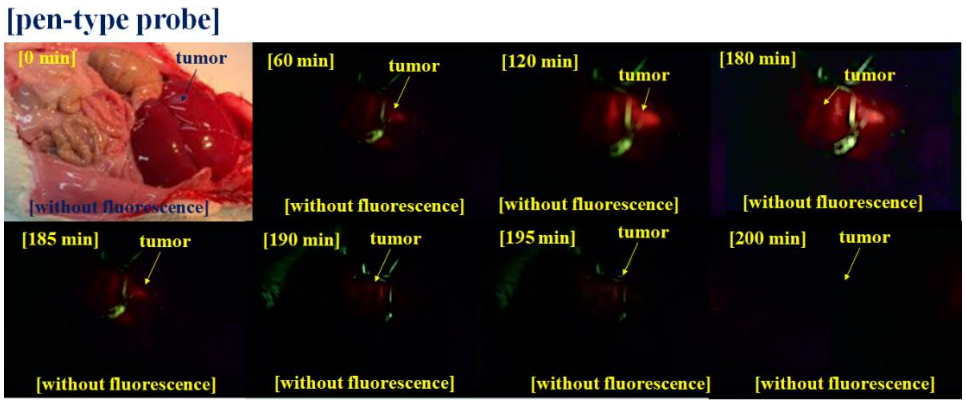

Preprints (www.preprints.org) | NOT PEER-REVIEWED | Posted: 21 April 2021 doi:10.20944/preprints202104.0573.v1

(c)

Figure 8. Experimental results of small animals (a) conventional surgical microscope (b) NIR camera (Lt-225 M/N) (c) pen-type probe camera.

4. Discussion

For the observation progress of 5-ALA fluorescence emission (see Fig. 8), the camera of the pen-type probe is compared with the NIR (lumenera Lt-225 M/N). The NIR camera is a candidate for black and white color imaging, and the pen-type probe's camera shows color imaging. The results of the pen-type probe's camera appears better than the others, as shown in Table 1.

Table 1. Comparison of the performance of pen-type probe's camera and others.

	Present work	**Lt-225**	**[18]**	**fluoptics [18]**	**[20]**	**[25]**
resolution [pixels]	1600×1200	2048×1088	1024×1024	720×576	800×600	256×512
frame rate [fps]	30	170	30	25	20	20
FOV [mm^2]	76×42	37.1×38.6	14.6×14.6	2.2×1.5	31.3×41.7	10×10
sensor	CMOS	CMOS	CMOS	CCD	CMOS	CCD

The resolution, frame, and pixel size of a pen-type probe camera (except for the NIR camera) is excellent (more than two times) and better than that obtained in previous studies [18, 20, 25]. In Fig. 10, the external irradiation optical source power (laser module) of a conventional surgical microscope was 55–160 mW/cm^2 [4], [15], [18], [25]-[29], and the working distance was 15–30 cm [4, 15, 18, 23, 25, 29]. However, the external irradiation optical intensity will have losses of approximately 58 % when the working distance is above the minimum of 200 mm [30].

To generate 5-ALA fluorescence emission, it is necessary to increase the optical source intensity or decrease the working distance. If the optical intensity of a laser module is increased, the laser module will be thermally broken because of the limitation of the laser module performance as the laser module is weak to heat, as shown experimentally. In addition, if the working distance of a conventional surgical microscope is decreased, the field of view (FOV) dimension is narrowed. Therefore, the viewing angle of lesion observation becomes very narrow [31, 32].

However, the pen-type probe LD can be sufficient for adjusting the LD power and working distance. As shown in Fig. 9, the LD and working distance of the pen-type probe are adjusted to 4 mW/cm^2 and 50 mm, respectively, and the FOV can be obtained as 60°. Thus, the tumor removal (or extant) condition is suitable for monitoring 5-ALA fluorescence emission. The conventional surgical microscope limits the adjustment range of the optical source power (55–169 mW/cm^2) and the working distance (15–30 cm). However, the optical source and working distance of the pen-type probe are freely adjustable. In addition, the photographing angle of a conventional surgical microscope has a maximum of 30° [33], and the photographing angle of the pen-type probe is free (360°) [34]-[37]. Therefore, the pen-type probe does not have a blind spot, and the pen-type probe's FOV angle broadens more than that of the the conventional one.

Preprints (www.preprints.org) | NOT PEER-REVIEWED | Posted: 21 April 2021 doi:10.20944/preprints202104.0573.v1

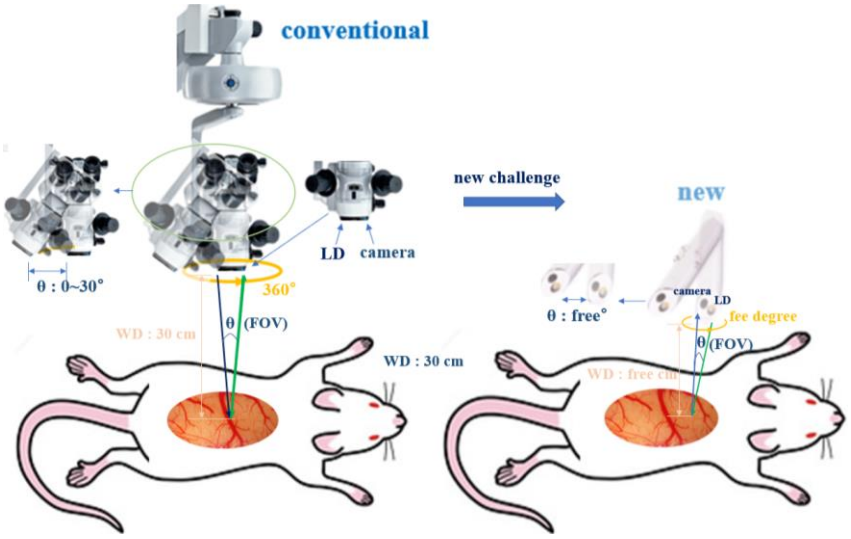

Figure 9. Comparison of performance for surgical microscope and a pen-type probe.

The conventional surgical microscope is bulky (6 kg) [20, 21], [23], and the surgical microscope must be supplied with electrical energy from an outside source. Thus, it is not portable, and the size of the operating room narrows owing to the large size of the microscope. However, the irradiation of the maximum power of an LD is 19 mW, and the actual LD power is within 4 mW. This was reduced by approximately 180 times. Thus, a pen-type probe can be operated using a battery. Therefore, the pen-type probe can be made small, and it is portable and can be used in a narrow operating room.

The characteristic of 5-ALA fluorescence contrast diagnosis has been formally approved by the US FDA [17, 18]. Therefore, it can be applied to the diagnosis of gliomas, brain cancer, breast cancer, colonic mucosa, and ovarian cancer [1]-[5].

5. Conclusions

A small and portable pen-type probe was proposed. It comprises a laser diode, an endoscope camera, a brightness control device of a light source, a power supply, and a communication contactor. The pen-type probe can be connected to an external monitor using a cable. Therefore, it can be used to observe tissues from the outside by using a monitor.

If a pen-type probe is used, the shape, color, and boundary of tumors and vasculature can be easily distinguished through fluorescence. It allows the adjustment of the beam direction and angle; therefore, free organizational observations are possible.

The pen-type probes are independent of the working distance. Thus, there is neither an optical density loss (about the working distance) nor a blind spot (about the view angle). Laser irradiation should be conducted within a safe range of tissues. The use of lasers should be in accordance with the international medical standards (IEC 60601-2-41). Small animal experiments were conducted at the Experimental Animal Center of Korea's Lee, Gil-Ya Cancer Diabetes Research Institute (IACUC No. LCDI-2017-0050).

For small animal experiments, the wavelength and power of the laser diode were 405 nm and 4.0 mW/cm^2, respectively. The fluorescence emission wavelength and power were 620–670 nm and 0.4 mW/cm^2, respectively. The fluorescence brightness duration reached a maximum of 180 min.

Author Contributions: design and simulation; K. C. Yoon, analysis and supervisor; KG. Kim, and clinical data collection, S. H. Lee. All authors have read and agreed to the published version of the manuscript.

Funding: This work was supported by the Gachon University Gil Medical Center (FRD2019-08) and Gachon Univ (2018-0669).

Institutional Review Board Statement: Not applicable.

Informed Consent Statement: Not applicable.

Data Availability Statement: The data presented in this study are available upon request from the corresponding author. The data are not publicly available because of privacy and ethical restrictions.

Acknowledgments: The experiment was an animal test from the "Experimental Animal Center of Korea's Lee, Gil-Ya Cancer Diabetes Research Institute" (IACAU No. : LCDI-2017-0050) through the permission of animal institutional review board (IRB) at animal ethics commission.

Conflicts of Interest: The authors declare no conflict of interest.

References

1. K. Mahmoudi, KL. Garvey, A. Bouras, G. Cramer, H. Stepp, JG. Jesu Raj, D. Bozec, TM. Busch, and CG. Hadjipanayis. 5-aminolevulinic acid photodynamic therapy for the treatment of high-grade gliomas. *J Neuro-oncology*, 2019 ; **141**, 595–607.
2. R. Yagi, S. Kawabata, N. Ikeda, N. Nonoguchi, M. Furuse, Y. Katayama, Y. Kajimoto, and T. Kuroiwa. Intraoperative 5-aminolevulinic acid-induced photodynamic diagnosis of metastatic brain tumors with histopathological analysis. *World J Surg Oncol*. 2017; **15**, 179.
3. T. Osaki, Y. Uto, M. Ishizuka, T. Tanaka, N. Yamanaka, T. Kurahashi, K. Azuma, Y. Murahata, T. Tsuka, N. Itoh, T. Imagawa, and Y. Okamoto. Artesunate Enhances the Cytotoxicity of 5-Aminolevulinic Acid-Based Sonodynamic Therapy against Mouse Mammary Tumor Cells In Vitro. *Molecules*., 2017; **22**, 533.
4. C Eker, S Montan, E Jaramillo, K Koizumi, C Rubio, S Andersson-Engels, K Svanberg, S Svanberg, and P Slezak. Clinical spectral characterisation of colonic mucosal lesions using autofluorescence and δ aminolevulinic acid sensitization. *Gut*. 1999; **44**, 511–518.
5. Y. Yokoyama, T. Shigeto, R. Miura, A. Kobayashi, M. Mizunuma, A. Yamauchi, M. Futagami, and H. Mizunuma. *Oncol Lett*. 2017; **13**, 4933–4938.
6. C. Malkanthi and M. B. Dissanayake. Brain tumor boundary segmentation of MR imaging using spatial domain image processing. *Int. J. for Innovation Education and Research*, 2017; **5**, 01-09.
7. N. Unno, M. Suzuki, N. Yamamoto, K. Inuzuka, D. Sagara, M. Nishiyama, H. Tanaka, and H. Konno. Indocyanine green fluorescence angiography for intraoperative assessment of blood flow: a feasibility study. *European J. Vasc. Endovasc. Surg*., 2008; **35**, 205-207.
8. T. Desmettre, J. M. Devoisselle, and S. Mordon. Fluorescence properties and metabolic features of indocyanine green (ICG) as related to angiography. *Elsevier Sci. Inc*., 2000; **45**, 15-27.
9. Handgraaf H, Boonstra M, Erkel A Van. Current and future intraoperative imaging strategies to increase radical resection rates in pancreatic cancer surgery. *Biomed Res*., 2014; 2014890230.
10. B. Qi, A. J. Crawford, N. E. Wojtynek, M. B. Holmes, J. J. Souchek, G. Almeida-Porada, Q. P. Ly, S. M. Cohen, M. A. Hollingsworth, and A. M. Mohs. Indocyanine green loaded hyaluronan-derived nanoparticles for fluorescence-enhanced surgical imaging of pancreatic cancer. *Nanomedicine: Nanotechnology, Biology, and Medicine*, 2018; **14**, 769–780.
11. T. Wada, K. Kawada, R. Takahashi, M. Yoshitomi, K. Hida, S. Hasegawa, Y. Sakai. ICG fluorescence imaging for quantitative evaluation of colonic perfusion in laparoscopic colorectal surgery. *Surg. Endosc*., 2017; **31**, 4184–4193.
12. G. M. Son, M. S. Kwon, Y. Kim, J. Kim, S. H. Kim, and J. W. Lee. Quantitative analysis of colon perfusion pattern using indocyanine green (ICG) angiography in laparoscopic colorectal surgery. *Surgical Endoscopy*, 2019; **33**, 1640–1649.
13. J. C. Delong, E. P. Ward, T. M. Lwin, K. T. Brumund, K. J. Kelly, S. Horgan, and M. Bouvet. Indocyanine green fluorescence-guided parathyroidectomy for primary hyperparathyroidism. *Surgery*; 2018; **163**, 388–392.
14. J. C. Yoo, S. P. Lee, J. G. Kim, G. H. Choi, H. T. Yeo. An image study of malignant glioma model with diffraction enhanced imaging computed tomography. *J. Korean Brain Tumor Society*, 2011; **10**, 103-109.
15. N. Y. Hong, H. R. Kim, H. M. Lee, D. K. Sohn, and KG Kim. Fluorescent property of indocyanine green (ICG) rubber ring using LED and laser light sources. Biomedical Optics Express, 2016; **7**, 1637-1644.
16. C. T. Wen, Y. Y. Liu, H. Y. Fang, M. J. Hsieh, and Y. K. Chao. Image-guided video-assisted thoracoscopic small lung tumor resection using near-infrared marking. Springer Surg. Endosc., 2018; **32**, 4673-4680.
17. C. G. Hadjipanayis and W. Stummer. 5-ALA and FDA approval for glioma surgery. *J. Neurooncol*. 2019; **141**, 479–486.
18. Clinical pharmacology and biopharmaceutics review (s), Center for Drucg Evaluation and Research (Application No. 208630 orig1s000).
19. GR Cherrick, SW Stein, CM Leevy. CS Davidson. Indocyanine green: Observation on its physical properties, plasma decay and hepatic extraction. *J. of Clin Invest*. 1960; **39**, 592-600.
20. J. R. Watson, C. F. Gainer, N. Martirosyan, J. Skoch, G. Michael Lemole, R. Anton, and M. Romanowski. Augmented microscopy: real-time overlay of bright-field and near-infrared fluorescence images. *J. of Biomedical Optica*, 2015; **20**, 106002.
21. H. R. Kim, H. M. Lee, H. Yoo, S. H. Lee, and KG Kim. Review of neurosurgical fluorescence imaging systems for clinical application. *J. of the Optical Society of Korea*. 2016; **20**, 305-313.
22. E. S. Molina, L. Stögbauer, A. Jeibmann, N. Warneke, and W. Stummer. Validating a new generation filter system for visualizing 5-ALA-induced PpIX fluorescence in malignant glioma surgery: a proof of principle study. **Acta Neurochirurgica**. 2020; **162**, 785–793.

23. J. F. Georges, A. Valeri, H. Wang, A. Brooking, M. Kakareka, S. S. Cho, Z. Al-Atrache, M. Bamimore, H, Osman, J. Ifrach, S. Yu, C. Li, D. Appelt, J. Y. K. Lee, P. Nakaji, K. Brill, and S. Yocom. Delta-aminolevulinic acid-mediated photodiagnoses in surgical oncology: a historical review of clinical trials. *Front. Surg*. 2019; **04**, 1-16.
24. W. Stummer, H. stepp, O. D. Wlestler, and U. Pichlmeler. Randomized, Prospective double-blinded study comparing 3 different doses of 5-Aminolevulinic acid for fluorescence-guided resections of malignant gliomas. *Neuro Surgery*. 2017; **81**, 230-239.
25. L. Ma and B. Li. Comprehensive review of surgical microscopes: technology development and medical applications. *J. of Biomedical Optics*, 2021; **26**, 010901 (1).
26. C. Detter, S. Wipper, D. Russ, A. Iffland, L. Burdorl, and E. Thein. Fluorescent cardiac imaging: a novel intraoperative method for quantitative assessment of myocardial perfusion during graded coronary artery stenosis. *Circulation*, 2007; **116**, 1007-14.
27. S. Wipper, B. Reiter, D. Russ, F. Hahnel, JF Kersten, and T. Kolbel. Distinction of non-ischemia inducing versus ischemia inducing coronary stenosis by fluorescent cardiac imaging. *Int. J. Cardiovasc Imaging*, 2016; 32, 363-71.
28. C. Detter, D. Russ, JF Kersten, H. Reichenspurner, and S. Wipper. Qualitative angiographic and quantitative myocardial perfusion assessment using fluorescent cardiac imaging during graded coronary artery bypass stenosis. *Int. J. Cardiovasc Imaging*. **2018**; 34, 159-167.
29. K. C. Yoon, EJ. Kim, KG. Kim, and SH Lee. A multi-detection microscope with 5-ALA and ICG Using dual array LED. *Current Optics Photonics*, **2019**; 3, 256-262.
30. P. Hoerenz, The operating microscope I. Optical principles illumination systems, and support systems. *J. of Microsurgery*, 1980; 1, 364-369.
31. P. Hoerenz. The operating microscope II. Individual parts, handling, assembling, focusing, and balancing. *J. of Microsurgery*, 1980; 1, 419-427.
32. L. Wei, D. W. Roberts, N. Sanai, and J. T. C. Liu. Visualization technologies for 5-ALA-based fluorescence-guided surgeries. *Journal of Neuro-Oncology*, 2019; **141**, 495–505.
33. J. Lee, R. E. Wijesinghe, D. Jeon, P. Kim, Y. H. Choung, J. H. Jang, M. Jeon, and J. Kim. Clinical utility of intraoperative tympanomastoidectomy assessment using a surgical microscope integrated with an optical coherence tomography. *Scientific Reports*. 2018; **8**, 1-8.
34. F. Ricci, F. Missiroli, L. Cerulli. Indocyanine green dye enhanced micro pulsed diode laser: a novel approach to subthreshold RPE treatment in a case of central serous chorioretinopathy. *European J. Ophthalmology*, 2003; **14**, 74-82.
35. M. V. Marshall, J. C. Rasmussen, I.-C. Tan, M. B. Aldrich, K. E. Adams, X. Wang, C. E. Fife, E. A. Maus, L. A. Smith, E. M. Sevick-Muraca. Near-infrared fluorescence imaging in humans with indocyanine green: a review and update. *Open Surgical Oncology Journal (Online)*, 2010; **2**, 12.
36. G. Themelis, J. S. Yoo, V. Ntziachristos. Multispectral imaging using multiple-bandpass filters. *Optics Lett*. 2008; 33, 1023-1025.
37. Y. Kondo, Y. Murayama, H. Konishi, R. Morimura, S. Komatsu, A. Shiozaki, Y. Kuriu, H. Ikoma, T. Kubota, M. Nakanishi. Fluorescent detection of peritoneal metastasis in human colorectal cancer using 5-aminolevulinic acid. *Int. J. Oncology*, 2014; **45**, 41-46.